Searching for Dark Matter with an Optical Cavity and an Unequal-Delay Interferometer

Etienne Savalle,[1] Aurélien Hees,[1] Florian Frank,[1] Etienne Cantin,[1] Paul-Eric Pottie,[1] Benjamin M. Roberts,[2] Lucie Cros,[1,3] Ben T. McAllister,[4] and Peter Wolf[1,*]

[1]*SYRTE, Observatoire de Paris, Université PSL, CNRS, Sorbonne Université, LNE, 75014 Paris, France*
[2]*School of Mathematics and Physics, The University of Queensland, Brisbane QLD 4072, Australia*
[3]*MINES ParisTech, Université PSL, 75006 Paris, France*
[4]*ARC Centre of Excellence for Engineered Quantum Systems, School of Physics, University of Western Australia, Crawley, Western Australia 6009, Australia*

(Received 11 June 2020; revised 9 December 2020; accepted 14 January 2021; published 4 February 2021)

We propose a new type of experiment that compares the frequency of a clock (an ultrastable optical cavity in this case) at time t to its own frequency some time t-T earlier, by "storing" the output signal (photons) in a fiber delay line. In ultralight oscillating dark matter (DM) models, such an experiment is sensitive to coupling of DM to the standard model fields, through oscillations of the cavity and fiber lengths and of the fiber refractive index. Additionally, the sensitivity is significantly enhanced around the mechanical resonances of the cavity. We present experimental results of such an experiment and report no evidence of DM for masses in the $[4.1 \times 10^{-11}, 8.3 \times 10^{-10}]$ eV region. In addition, we improve constraints on the involved coupling constants by one order of magnitude in a standard galactic DM model, at the mass corresponding to the resonant frequency of our cavity. Furthermore, in the model of relaxion DM, we improve on existing constraints over the whole DM mass range by about one order of magnitude, and up to 6 orders of magnitude at resonance.

DOI: 10.1103/PhysRevLett.126.051301

Introduction.—Dark matter (DM) remains one of the contemporary mysteries in fundamental physics and continues to question the scientific community regarding its origin and composition. DM leaves indirect evidences of its existence through its gravitational interaction but has never been directly detected so far [1], leading to the development of a multitude of experiments probing different models covering a large mass range [1,2].

Amongst the various DM models, ultralight DM scenarios have recently seen a strong surge thanks to the excellent sensitivities provided by the latest advances in time and frequency metrology [3–16]. In such class of models, DM is made of a scalar field (SF) nonuniversally coupled to the standard model. Typically, this SF will undergo oscillations that will be reflected through an oscillation of the fundamental constants of nature, a signature of a violation of the equivalence principle. This has motivated experimental searches for harmonic variations of the constants of nature in a wide range of frequencies: with atomic clocks in the 10^{-10}–1 Hz region [6,7,16], with a network of optical cavities in the 10^{-4}–10^{-1} Hz region [11], and using atomic spectroscopy in the 10^{5}–10^{8} Hz region [17]. This has also given rise to various proposals for experiments to further extend the frequency range of searches for oscillations in the constants of nature: using a future atomic gravitational waves detector in the 10^{-3}–10^{3} Hz region [18], using future resonnant-mass detectors in the 10^{4}–10^{6} Hz region [19], using a laser gravitational waves detector in the 10^{-2}–10^{2} Hz region [20–22], etc. In this Letter, we propose a new type of experiment consisting of a three-arm Mach-Zender interferometer (see also the preprint [23]) to search for harmonic variations in the fine-structure constant and in the mass of the electron in the partially unexplored 10^{4}–10^{6} Hz region. Furthermore, we present results from an experimental realization developed at the Paris Observatory that provides the first constraints in the oscillations of the constants of nature in the 10^{4}–10^{5} Hz frequency range and improves over previous results [17] in the 10^{5}–10^{6} Hz frequency range. Finally, we present an interpretation of these experimental results for different scenarios of DM.

Ultralight scalar field oscillation.—The theory of an ultralight SF has been developed in, e.g., Refs. [4,5,24]. Within this framework, a scalar field φ of mass m_φ is linearly coupled to the standard model Lagrangian leading to space-time variations of any fundamental constant X from the standard model. The coupling parameters d_X characterize the strength of the interaction between the SF and the various sectors of the standard model. More precisely, they parametrize the variation of the constants of nature [24] such that $X(\varphi) = X_0(1 + d_X\varphi)$ where X denotes any constant of nature like, e.g., the fine structure constant $\{\alpha, d_e\}$, the mass of fermions $\{m_j, d_{m_j}\}$ ($j =$ electron, quarks), and the QCD mass scale $\{\Lambda_{\mathrm{QCD}}, d_g\}$, and the subscript 0 refers to the value of the constant in absence of the SF.

In this Letter, we will focus on low SF masses ($m_\varphi \ll 1$ eV) for which φ behaves as a classical field. This SF admits oscillating solutions $\varphi = \varphi_0 \cos(\omega_m t)$ (with ω_m the SF Compton-De Broglie frequency) [4,5,7] which induces a temporal evolution of the constants of nature. When the SF is interpreted as DM, its amplitude of oscillation is directly related to the local DM density $\rho_{\rm DM}$ (0.4 GeV/cm^3 in the standard galactic halo DM model [25]). Variations of the fine structure constant and/or electron mass results in a variation of atomic transition frequencies and of the Bohr radius $a_0 = \hbar/(m_e c\alpha)$, which in turn leads to variation of the frequency of atomic clocks and the length of solids. This has motivated several experimental searches for harmonic variations of the constants of nature using various atomic experiments [2].

In addition, searches for a Yukawa-like violation of the universality of free fall also provide constraints on the couplings between matter and the SF, see, e.g., Refs. [10,26,27]. Those constraints are independent of the identification of the SF as DM (and are therefore independent of the relative abundance and of the composition of DM).

Experimental setup.—Our experimental setup, dubbed the DAMNED (DArk Matter from Non Equal Delays) experiment is a three-arm Mach-Zender interferometer [23] as shown in Fig. 1. A 1542 nm laser source is stabilized on an ultrastable cavity [28,29], with a locking bandwidth of a few 100 kHz. The beam power is then unevenly distributed between the three arms. Most of the power is going through the long delay line that consists of a fiber spool (52 or 56 km) with a refractive index $n_0 \approx 1.5$. To perform a self-heterodyne detection, the laser frequency is shifted with the acousto-optic modulator (AOM) located in the second arm (where $\nu_{\rm AOM} \approx 37$ MHz). Finally, the last arm is a one meter fiber.

The beat note between the AOM and the fiber spool arms provides the putative DM signal resulting from the beat between the (DM induced oscillating) cavity frequency at time t and its frequency at time t-T as seen through the fiber with delay T (see next section for details). The reference beat note between the AOM and the short fiber provides an indication of the experimental perturbations (noise and systematics) as the arm length is too short to see any cavity frequency oscillations. Both beat notes are acquired simultaneously using a digital two channel phase meter (Ettus X310) that provides the phase measurements (after demodulation of the 37 MHz signal) at a sampling rate of 500 kHz.

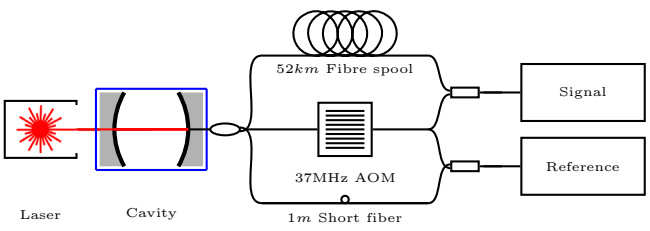

FIG. 1. Experimental setup. A 1542 nm laser source is locked to an ultrastable cavity. The beam is then split between three arms and recombined to have access to the DM signal (long vs AOM arms) and the experimental reference (short vs AOM arms).

Impact of an oscillating scalar field on the experiment.—An oscillating scalar field will impact two parts of our experiment. First, it will lead to oscillations of the cavity frequency $\omega(t)$ due to variations of its length induced by oscillations of the Bohr radius. Second, the fiber delay $T(t)$ will oscillate because of variations of its length and of its refraction index that are both induced by oscillations of the constants of nature.

The laser is locked to an optical resonance of the cavity. The variation of the frequency of the light exiting the cavity $\delta\omega(t)$ is then proportional to its length variation and is given by

$$\frac{\delta\omega(t)}{\omega_0} = \epsilon_L[\mathcal{E}_c(1+\alpha)\cos(\omega_m t) + \mathcal{E}_s\beta\sin(\omega_m t)], \quad (1)$$

where ω_0 is the unperturbed cavity frequency, $\epsilon_L = \varphi_0(d_e + d_{m_e})$ is the fractional length change due to oscillations of the Bohr radius. The coefficients $\mathcal{E}_c$ and $\mathcal{E}_s$ characterize the optical properties of the cavity. For our high finesse cavity ($\mathcal{F} \approx 800000$ [28]) and frequencies of interest ($f \in [10, 200]$ kHz), we have $\mathcal{E}_c, \mathcal{E}_s \simeq 1$. On the other hand, the α and β coefficients characterize the mechanical properties of the cavity. For our ~0.1 m ultra low expansion cavity the mechanical resonant frequencies are $\omega_n = 2\pi n 27.6$ kHz where n is an integer ($n \geq 1$), and are therefore well within our frequency region of interest ([10, 200] kHz). Only odd resonances are excited due to the symmetry of the length change. At resonance ($\omega_m = \omega_1$), $\alpha \simeq 0$ and $\beta = 8Q_1/\pi^2$, with the quality factor of our ultra low expansion cavity $Q_1 = 6.1 \times 10^4$ [28,30,31] which significantly enhances the signal searched for. Below resonance ($\omega_m \ll \omega_1$) both $\beta, \alpha \simeq 0$. A detailed derivation of the coefficients $\alpha, \beta, \mathcal{E}_c, \mathcal{E}_s$ is provided in the Supplemental Material [32]. A similar analysis was also carried out in Refs. [19,22] giving similar results. Note that the mechanical resonant frequencies and Q factors are determined from material dependent constants (see Ref. [32]) and we conservatively assume a 5% uncertainty in those constants.

The fiber delay is given by $T(t) = L_f(t)n(t)/c$, where $L_f(t)$ and $n(t)$ are the fiber length and refractive index, respectively, both of which oscillate due to the variations of the constants of nature. Using the approach described in Ref. [42], we find

$$\frac{\delta T(t)}{T_0} = \frac{\omega_0}{n_0}\frac{\partial n}{\partial \omega}\left(\frac{\delta\omega(t)}{\omega_0} - \epsilon_n\cos(\omega_m t)\right) - \epsilon_L\cos(\omega_m t), \quad (2)$$

where $\delta\omega(t)/\omega_0$ is the relative frequency variation at the entrance of the fiber, which in our case is given by Eq. (1)

and ϵ_n is the fractional refractive index change that is directly proportional to the amplitude of oscillations of the SF through

$$\epsilon_n = \varphi_0[2d_e + d_{m_e} + (d_{m_e} - d_g)/2 - 0.024(d_{m_q} - d_g)]. \tag{3}$$

The dependence on d_g and d_{m_q} arises from the phonon frequencies in the fiber that determine its refractive index [42]. For the telecom fibers that we use the prefactor of Eq. (2) is typically $\approx 10^{-2}$.

Both the cavity frequency and fiber delay oscillations can be integrated to obtain the phase difference $\Delta\Phi(t)$ between the delayed and nondelayed signals:

$$\begin{aligned}\Delta\Phi(t) &= \int_{t-T_0-\delta T(t)}^{t} [\omega_0 + \delta\omega(t')]dt' \\ &= \omega_0 T_0 + 2\frac{\omega_0}{\omega_m}\sin\left(\frac{\omega_m T_0}{2}\right)\left[C_{\Delta\Phi}\cos\left(\omega_m t - \omega_m\frac{T_0}{2}\right)\right. \\ &\quad \left. + S_{\Delta\Phi}\sin\left(\omega_m t - \omega_m\frac{T_0}{2}\right)\right],\end{aligned} \tag{4}$$

where $C_{\Delta\Phi}$ and $S_{\Delta\Phi}$ are derived from Eqs. (1) and (2), to leading order:

$$C_{\Delta\Phi} \simeq \epsilon_L\alpha - \epsilon_n\frac{\omega_0}{n_0}\frac{\partial n}{\partial\omega}; \qquad S_{\Delta\Phi} \simeq \epsilon_L\beta. \tag{5}$$

Since Eq. (4) has extinctions for $\omega_m T_0 = n2\pi$, we use two different fiber lengths (thus two different delays T_0) to recover sensitivity over the whole desired frequency range. For the reference arm $T_0 \simeq 0$, and the signal of Eq. (4) vanishes, which allows its use to characterize systematic effects and identify false DM signals.

Experimental results.—The parallel acquisitions of the signal and reference phase data lasted 12 days each for the two different fiber lengths (52.64 and 56.09 km) at a 500 kHz sampling rate. The total raw phase data ($\sim 4 \times 2.1$ TB) requires digital preprocessing to compute Fourier transforms with a spectral resolution limited to ~ 3 mHz [43].

Figure 2 shows the power spectral density (PSD) computed over the full 12 days duration of the experiment. Only the "signal" branch for the 52 km acquisition is shown here, but all results are similar for the 56 km fiber, as well as for the "reference" branch. One can see characteristic "bumps" arising from the cavity noise seen through the transfer function of our unequal-length arm interferometer [32]. Our experimental sensitivity is limited below 10 kHz by the acoustic and thermal noise of the long signal fiber and above 200 kHz by the bandwidth of the phase-locked loop that locks the laser to the cavity (which we optimised in our experiment to $\approx$500 kHz). In between, the experiment is limited by the cavity noise floor which was

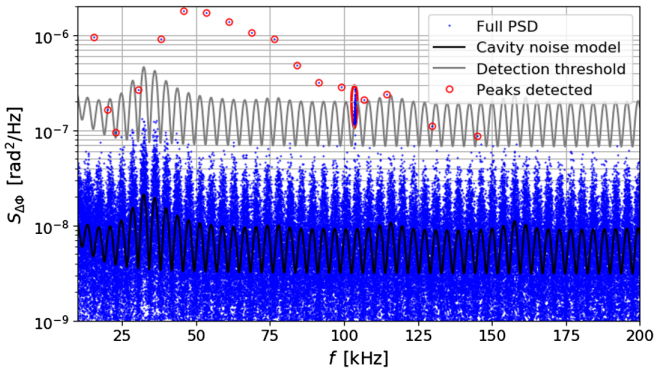

FIG. 2. PSD of phase fluctuations $S_{\Delta\Phi}(f)$ of the signal for the 52 km fiber (in blue). The modeled cavity noise floor is shown in black, with the grey line indicating the 95% detection threshold [44] which reveals several significant peaks (in red).

stationary during the full duration of both acquisitions. The modeled cavity noise is an averaged PSD over 268 s data subsets and is required later for our statistical analysis (see Ref. [32] for details).

Systematic effects.—In order to identify a potential DM signal, we investigate any signal (peak in the PSD) emerging from the noise. For this, we use the method presented in Ref. [44] to define a detection level above which any peak can be considered as a real signal with a false detection rate lower than 5%. As one can see in Fig. 2, the detection threshold (grey line), is exceeded by many peaks (red dots). At closer inspection (see Ref. [32] for details) all of these peaks turn out to be systematic effects that are either present only in the cavity used for the experiment and not in the other cavities available in the laboratory, and/or are correlated to temperature changes in the laboratory, or are also present in the reference branch which is insensitive to coupling with DM. Additionally, they have a spectral shape and width incompatible with the signal in the DM models we consider. Therefore, we report no detection of ultralight DM in the frequency range $[10, 200]$ kHz. However, that conclusion does not apply at the frequencies of the systematic peaks, which might mask a putative DM signal, and we thus exclude those frequency regions from our results, as summarized in Table I. All the peak positions are drifting

TABLE I. Excluded frequency regions due to systematic effects.

Origin	$\langle f\rangle$/Hz	r_f	σ_f/Hz	[$f_{\min}$/Hz,	$f_{\max}$/Hz]
Unknown	26178	10^{-4}	1	[26172.382,	26183.618]
	50069	10^{-4}	1	[50060.993,	50077.007]
	59364	10^{-4}	1	[59355.064,	59372.936]
Piezo	101684	10^{-3}	3	[101573.316,	101794.684]
	103525	10^{-3}	3	[103412.975,	103638.025]
Ettus	Multiples of 7629.395 Hz, $\sigma_f = 3$ mHz				

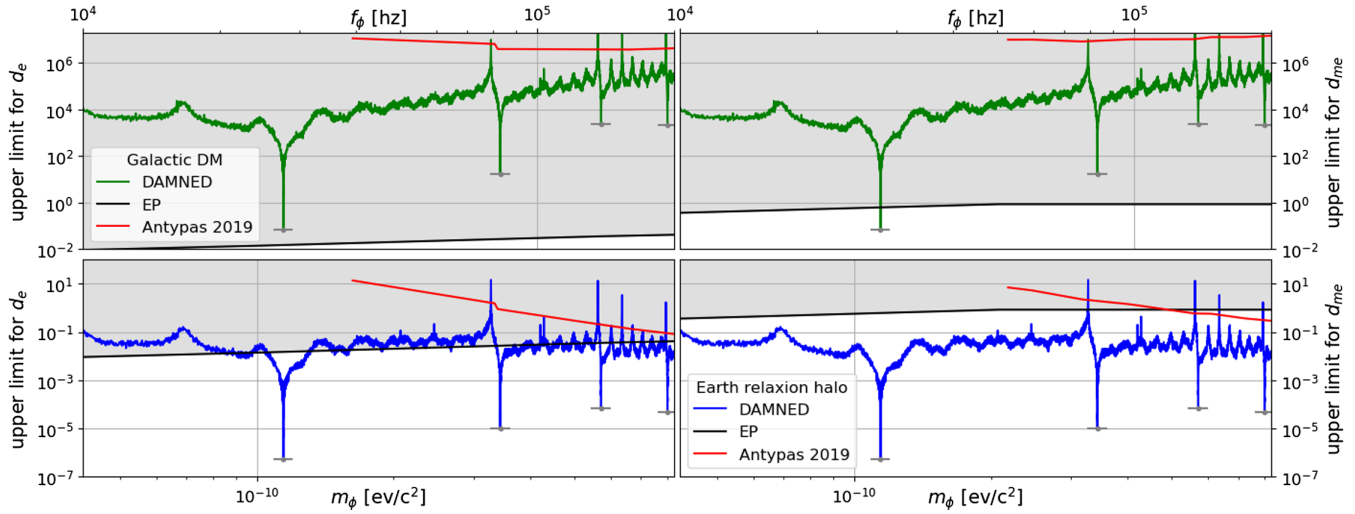

FIG. 3. 95% confidence upper limits on d_e and d_{m_e} in the usual galactic DM model (top) and in the Earth relaxion halo one (bottom). Sensitivity peaks are at the mechanical resonance frequencies of the cavity. The solid black line corresponds to the constraints set by the Eöt-Wash torsion balance experiments [10,26,49] while the red line corresponds to a more recent experiment [17]. Narrow frequency bands excluded from these constraints because of systematic effects are given in Table I. Note that the frequency and amplitude of the resonance peaks may differ from those shown by ~5% because of the uncertainty in ω_n and Q_n, as indicated by the grey error bars.

relatively to their mean value $\langle f \rangle$ by a factor r_f. With the peak widths σ_f, we define a conservative exclusion interval $[\langle f \rangle \times (1 - r_f) - 3\sigma_f, \langle f \rangle \times (1 + r_f) + 3\sigma_f]$.

Constraints on ultralight dark matter.—The first DM model for which we interpret our measurements is a standard model where all the DM density is assumed to be uniformly distributed in the solar system and is carried by the scalar field [4,5,10]. In standard models of galaxy formation, galactic DM must be virialized [45,46] and has a velocity distribution $f_{\rm DM}(v)$ with a characteristic width $\sigma_v \sim 10^{-3}c$ [33,34,47]. The Compton frequency of the SF, $\omega_m \simeq m_\varphi c^2/\hbar[1 + v^2/(2c^2)]$, is broadened because of the DM velocity distribution. This broadening introduces a coherence time $\tau_c = (\omega_m \sigma_v^2/c^2)^{-1} \sim 10^6 \omega_m^{-1}$ [48]. The DM distribution therefore implies that the scalar field has a stochastic component from the sum of all the SF allowed by the velocity distribution. The effective field takes the following form [34,35]:

$$\varphi(t) = \frac{\sqrt{\frac{4\pi\rho_{\rm DM}}{c^2}}}{\frac{m_\varphi c^2}{\hbar}} \sum_{j=1}^{N_j} \alpha_j \sqrt{f_{\rm DM}(f_j)\Delta f} \cos\left[2\pi f_j t + \phi_j\right], \quad (6)$$

where α_j are stochastic amplitudes following a Rayleigh distribution [34,35], ϕ_j are random phases following a uniform distribution, and $f_{\rm DM}(f)$ is the DM velocity distribution expressed in the frequency domain (see Refs. [32] and [33]). N_j defines the number of points used to discretize the DM frequency distribution curve ($N_j \Delta f \geq 1/\tau_c$, where Δf is the frequency resolution of the data). When the experimental duration $T_{\rm exp}$ is longer than τ_c, this stochastic broadening needs to be taken into account in the data analysis [33,34] and actually provides a useful handle on identifying the signal due to its peculiar spectral shape. Even when $T_{\rm exp} \leq \tau_c$, the stochastic nature of the signal needs to be taken into account as in general it leads to reduced sensitivity by up to 3 orders of magnitude because of the possibility of the instantaneous local oscillation amplitude being smaller than the average value which is related to $\rho_{\rm DM}$ [35].

In order to constrain the DM model, the coupling constants must be extracted from the coefficients $C_{\Delta\Phi}$ and $S_{\Delta\Phi}$ available in the Fourier transform of our data. The stochastic nature of the signal Eq. (6) requires the adjustment of the following parameters: the coupling constants d_X, N_j, amplitudes α_j, and N_j phases ϕ_j, where N_j is chosen to sufficiently sample the DM frequency distribution $f_{\rm DM}$. The *a priori* knowledge of the probability distribution of amplitudes (Rayleigh distribution) and phases (uniform distribution) favors the use of a Bayesian approach. Working in the frequency domain the corresponding posterior distributions can be analytically marginalized over the N_j amplitudes α_j and phases ϕ_j, which makes the problem numerically solvable (see Refs. [33–35] and Ref. [32]). The result is a posterior probability distribution for the coupling constants d_X for each DM mass, providing the corresponding 95% upper limit. To simplify, we concentrate on d_e and d_{m_e} and assume that only one of them is nonzero in turn, a so called "maximum reach approach." We use our acquisitions with two different fiber lengths and combine both likelihoods to infer a unique upper limit at 95% confidence. These upper limits for the galactic DM model (where we assumed that the scalar field is made from 100% of the DM energy density) are presented in the top part of Fig. 3. The constraints show large "peaks" at the resonant frequencies ($n = 1, 3, 5, 7$) of our cavity, and at frequencies

where the combination of two different fiber lengths does not fully solve the loss of sensitivity due to the $\sin(\omega_m T_0/2)$ term in Eq. (4). In between the peaks the constraints come from a combination of the length and index changes of the cavity and the fibers. For this specific theoretical scenario, our experiment exceeds best existing constraints on d_{m_e} from torsion balance experiments [10,26,49] by about an order of magnitude only over a narrow-frequency band around the cavity resonance, but broadly improves on the recent experiment reported in Ref. [17], by up to 3 orders of magnitude [50].

Constraints on the relaxion halo model.—The second theoretical model for which we interpret our experimental results is called the relaxion halo model [36]. In this scenario, DM forms a relaxion halo around the Earth [51–55] leading to a local overdensity with respect to the galactic DM density that depends on m_φ and can reach $\rho_{\rm RH}/\rho_{\rm DM} \leq 10^{16}$ in the range of m_φ considered here [36]. Additionally the velocity distribution, and therefore the coherence time, is modified, leading to $\tau_c \sim 10^{20}\omega_m^{-1}(2\pi{\rm Hz}/\omega_m)^2$. Both of these modifications have to be taken into account in the data analysis. First experimental searches in this model were reported in Refs. [17,37]. We present the constraint on the coupling parameters obtained in this scenario in the bottom of Fig. 3. In this model, our experiment improves on best existing constraints for almost all of the probed DM masses. That improvement reaches 5 orders of magnitude for d_e and 6 orders of magnitude for d_{m_e} at the mechanical resonances.

The underlying reason for the difference in sensitivity in the two models comes from the fact that experiments like ours or Ref. [17] depend on the local DM density while torsion balance experiments search for a Yukawa interaction between the Earth and the test masses, which is independent of the identification of the SF as DM [10] and are thus independent of the local DM density and composition.

In all cases our experiment improves on the recent experiment reported in Ref. [17], which directly probes the same DM models as ours, by typically 2–3 orders of magnitude over the DM mass region where the two overlap.

Conclusion.—In this Letter, we propose a new experiment to search for harmonic variation of the constants of nature at high frequencies. In addition, we present results from the DAMNED experiment developed at the Paris Observatory. This experiment has not revealed any sign of scalar DM for masses in the $[4.1 \times 10^{-11}, 8.3 \times 10^{-10}]$ eV region, but we have improved existing bounds on the DM-standard model coupling constants by amounts depending on the considered mass and DM distribution model.

Our main limitation is the cavity noise, and we plan to improve on the results presented here over the next years, and also test other models (e.g., axion couplings), using similar setups but with an improved optical cavity currently under construction.

Helpful discussions with Andrei Derevianko and Yevgeny Stadnik are gratefully acknowledged.

*peter.wolf@obspm.fr

[1] G. Bertone and T. M. P. Tait, Nature (London) **562**, 51 (2018).
[2] M. S. Safronova, D. Budker, D. DeMille, D. F. Jackson Kimball, A. Derevianko, and C. W. Clark, Rev. Mod. Phys. **90**, 025008 (2018).
[3] A. Derevianko and M. Pospelov, Nat. Phys. **10**, 933 (2014).
[4] A. Arvanitaki, J. Huang, and K. Van Tilburg, Phys. Rev. D **91**, 015015 (2015).
[5] Y. V. Stadnik and V. V. Flambaum, Phys. Rev. Lett. **115**, 201301 (2015).
[6] K. Van Tilburg, N. Leefer, L. Bougas, and D. Budker, Phys. Rev. Lett. **115**, 011802 (2015).
[7] A. Hees, J. Guéna, M. Abgrall, S. Bize, and P. Wolf, Phys. Rev. Lett. **117**, 061301 (2016).
[8] P. Wcisło, P. Morzyński, M. Bober, A. Cygan, D. Lisak, R. Ciuryło, and M. Zawada, Nat. Astron. **1**, 0009 (2016).
[9] B. M. Roberts, G. Blewitt, C. Dailey, M. Murphy, M. Pospelov, A. Rollings, J. Sherman, W. Williams, and A. Derevianko, Nat. Commun. **8**, 1195 (2017).
[10] A. Hees, O. Minazzoli, E. Savalle, Y. V. Stadnik, and P. Wolf, Phys. Rev. D **98**, 064051 (2018).
[11] P. Wcisło, P. Ablewski, K. Beloy, S. Bilicki, M. Bober, R. Brown, R. Fasano, R. Ciuryło, H. Hachisu, T. Ido, J. Lodewyck, A. Ludlow, W. McGrew, P. Morzyński, D. Nicolodi, M. Schioppo, M. Sekido, R. Le Targat, P. Wolf, X. Zhang, B. Zjawin, and M. Zawada, Sci. Adv. **4**, eaau4869 (2018).
[12] B. M. Roberts and A. Derevianko, arXiv:1803.00617.
[13] B. M. Roberts, G. Blewitt, C. Dailey, and A. Derevianko, Phys. Rev. D **97**, 083009 (2018).
[14] R. Alonso, D. Blas, and P. Wolf, J. High Energy Phys. 07 (2019) 069.
[15] P. Wolf, R. Alonso, and D. Blas, Phys. Rev. D **99**, 095019 (2019).
[16] C. J. Kennedy, E. Oelker, J. M. Robinson, T. Bothwell, D. Kedar, W. R. Milner, G. E. Marti, A. Derevianko, and J. Ye, Phys. Rev. Lett. **125**, 201302 (2020).
[17] D. Antypas, O. Tretiak, A. Garcon, R. Ozeri, G. Perez, and D. Budker, Phys. Rev. Lett. **123**, 141102 (2019).
[18] A. Arvanitaki, P. W. Graham, J. M. Hogan, S. Rajendran, and K. Van Tilburg, Phys. Rev. D **97**, 075020 (2018).
[19] A. Arvanitaki, S. Dimopoulos, and K. Van Tilburg, Phys. Rev. Lett. **116**, 031102 (2016).
[20] Y. V. Stadnik and V. V. Flambaum, Phys. Rev. A **93**, 063630 (2016).
[21] S. Morisaki and T. Suyama, Phys. Rev. D **100**, 123512 (2019).
[22] H. Grote and Y. V. Stadnik, Phys. Rev. Research **1**, 033187 (2019).
[23] E. Savalle, B. M. Roberts, F. Frank, P.-E. Pottie, B. T. McAllister, C. Dailey, A. Derevianko, and P. Wolf, arXiv:1902.07192.

[24] T. Damour and J. F. Donoghue, Phys. Rev. D **82**, 084033 (2010).
[25] P. J. McMillan, Mon. Not. R. Astron. Soc. **414**, 2446 (2011).
[26] T. A. Wagner, S. Schlamminger, J. H. Gundlach, and E. G. Adelberger, Classical Quantum Gravity **29**, 184002 (2012).
[27] J. Bergé, P. Brax, G. Métris, M. Pernot-Borràs, P. Touboul, and J.-P. Uzan, Phys. Rev. Lett. **120**, 141101 (2018).
[28] J. Millo, D. V. Magalhães, C. Mandache, Y. Le Coq, E. M. L. English, P. G. Westergaard, J. Lodewyck, S. Bize, P. Lemonde, and G. Santarelli, Phys. Rev. A **79**, 053829 (2009).
[29] X. Xie, R. Bouchand, D. Nicolodi, M. Lours, C. Alexandre, and Y. L. Coq, Opt. Lett. **42**, 1217 (2017).
[30] K. Numata, A. Kemery, and J. Camp, Phys. Rev. Lett. **93**, 250602 (2004).
[31] J. Zhang, Y. Luo, B. Ouyang, K. Deng, Z. Lu, and J. Luo, Eur. Phys. J. D **67**, 46 (2013).
[32] See Supplemental Material at http://link.aps.org/supplemental/10.1103/PhysRevLett.126.051301 for the detailed calculation of the cavity mechanical resonance and cavity optical resonance, for the cavity noise floor and for a detailed presentation of the statistical approach used in this analysis, which includes Refs. [17,19,22,28,29,33–41].
[33] A. Derevianko, Phys. Rev. A **97**, 042506 (2018).
[34] J. W. Foster, N. L. Rodd, and B. R. Safdi, Phys. Rev. D **97**, 123006 (2018).
[35] G. P. Centers, J. W. Blanchard, J. Conrad, N. L. Figueroa, A. Garcon, A. V. Gramolin, D. F. J. Kimball, M. Lawson, B. Pelssers, J. A. Smiga, A. O. Sushkov, A. Wickenbrock, D. Budker, and A. Derevianko, arXiv:1905.13650.
[36] A. Banerjee, D. Budker, J. Eby, H. Kim, and G. Perez, Commun. Phys. **3**, 1 (2020).
[37] S. Aharony, N. Akerman, R. Ozeri, G. Perez, I. Savoray, and R. Shaniv, arXiv:1902.02788.
[38] Y.-J. Lee, in *Physics III: Vibrations and Waves. Part 1: Mechanical Vibrations and Waves*, edited by MIT, 8.03SC (Massachusetts Institute of Technology, 2016), https://ocw.mit.edu.
[39] Virgo-Collaboration, *The VIRGO Physics Book, Vol. II, OPTICS and Related TOPICS* (The Virgo Collaboration, 2010), https://labcit.ligo.caltech.edu/~hiro/docs/vpb2.pdf.
[40] B. Canuel, A. Bertoldi, L. Amand, E. Borgo di Pozzo, B. Fang, R. Geiger, J. Gillot, S. Henry, J. Hinderer, D. Holleville, G. Lefèvre, M. Merzougui, N. Mielec, T. Monfret, S. Pelisson, M. Prevedelli, S. Reynaud, I. Riou, Y. Rogister, S. Rosat, E. Cormier, A. Landragin, W. Chaibi, S. Gaffet, and P. Bouyer, Sci. Rep. **8**, 14064 (2018).
[41] A. Banerjee, D. Budker, J. Eby, V. V. Flambaum, H. Kim, O. Matsedonskyi, and G. Perez, J. High Energy Phys. 09 (2020) 004.
[42] C. Braxmaier, O. Pradl, H. Müller, A. Peters, J. Mlynek, V. Loriette, and S. Schiller, Phys. Rev. D **64**, 042001 (2001).
[43] RAM limitation reduces the maximum amount of data duration that can be loaded to ∼268 s. The maximum spectral resolution is therefore $1/T_{\mathrm{RAM}} > 1/T_{\mathrm{exp}}$.
[44] J. D. Scargle, Astrophys. J. **263**, 835 (1982).
[45] K. Freese, M. Lisanti, and C. Savage, Rev. Mod. Phys. **85**, 1561 (2013).
[46] A. Pillepich, M. Kuhlen, J. Guedes, and P. Madau, Astrophys. J. **784**, 161 (2014).
[47] N. W. Evans, C. A. J. O'Hare, and C. McCabe, Phys. Rev. D **99**, 023012 (2019).
[48] A. Derevianko, Phys. Rev. A **97**, 042506 (2018).
[49] S. Schlamminger, K.-Y. Choi, T. A. Wagner, J. H. Gundlach, and E. G. Adelberger, Phys. Rev. Lett. **100**, 041101 (2008).
[50] Note that in Ref. [17] the authors do not take the factor ∼10 sensitivity loss pointed out in Ref. [35] into account, contrary to our work (see Ref. [32]).
[51] E. W. Kolb and I. I. Tkachev, Phys. Rev. Lett. **71**, 3051 (1993).
[52] D. G. Levkov, A. G. Panin, and I. I. Tkachev, Phys. Rev. Lett. **121**, 151301 (2018).
[53] E. Braaten and H. Zhang, Rev. Mod. Phys. **91**, 041002 (2019).
[54] A. Vaquero, J. Redondo, and J. Stadler, J. Cosmol. Astropart. Phys. 04 (2019) 012.
[55] B. Bar-Or, J.-B. Fouvry, and S. Tremaine, Astrophys. J. **871**, 28 (2019).